Fabrication of H$_2$S gas sensors using Zn$_x$Cu$_{1-x}$Fe$_2$O$_4$ nanoparticles

Mohammad Abu Haija[1] · Mariem Chamakh[2] · Israa Othman[1] · Fawzi Banat[3] · Ahmad I. Ayesh[2,4]

Abstract

Spinel ferrite nanoparticles can be easily retrieved and utilized for multiple cycles due to their magnetic properties. In this work, nanoparticles of a Zn$_x$Cu$_{1-x}$Fe$_2$O$_4$ composition were synthesized by employing a sol–gel auto-combustion technique. The morphology, composition, and crystal structure were examined using scanning electron microscopy, infrared spectroscopy, and X-ray diffraction. The produced nanoparticles are in the range of 30–70 nm and manifest spinel cubic structure. The nanoparticles were tested for their sensitivity to H$_2$ and H$_2$S gases, and the Cu-based spinel ferrite nanoparticles were found the most sensitive and selective to H$_2$S gas. Their enhanced response to H$_2$S gas was attributed to the production of metallic CuFeS$_2$ that manifest higher electrical conductivity as compared with CuFe$_2$O$_4$. The fabricated sensors are functional at low temperatures, and consequently, they need low operational power. They are also simple to fabricate with appropriate cost.

Keywords Spinel ferrite · CuFe$_2$O$_4$ · ZnFe$_2$O$_4$ · H$_2$S · Gas sensor · Nanoparticles

1 Introduction

Hydrogen sulfide (H$_2$S) gas pollution is considered a crucially poisonous to humans, especially at locations with high production yield such as petroleum extraction, refining, and transportation facilities [1]. It is distinguished with its odor that smells like a rotten egg that is well known at mineral water of thermal springs [2]. The development of efficient sensors is vital for environment monitoring and control in fields that involve H2S emission. Recently, there have been major achievements in the field of gas sensing by different systems including nanomaterials, nanoclusters, and graphene-based materials [3–5].

Nanoparticles consist of groups of atoms with nanometer size, and their chemical and physical properties are unlike their bulk counterparts [6]. Their nanometer size leads to a large percentage of surface atoms that represent active chemical reactive sites [6, 7]. Exposure of nanoparticles to a reactive gas causes its adsorption on the surface sites, thus, change the density of free electrons. As a result, the electrical current signal through a network of nanoparticles is modified [8, 9]. Such a modification in the current signal can be utilized to measure the amount of reactive gas. Conductometric gas sensors are devices that contain networks of nanoparticles that are sensitive and selective to certain gases, and their response signals are measured as the changes in electrical conductance. Those sensors are functional at low gas concentrations and feasible to fabricate with reasonable production cost [10–12].

Metal-oxide nanoparticles are known for their functionality in the field of gas sensing because of gas adsorption on their surfaces that leads to release of free electrons [13, 14]. Spinel ferrite nanoparticles are of a particular interest for gas sensors. Ferrites exhibit a general composition of MFe$_2$O$_4$, where *M* can be a metal atom such as Cu, Zn, and Ni. Utilization of spinel ferrite nanoparticles for device applications promotes materials' recycling because of their magnetic properties that enable their recovery. Copper and zinc spinel ferrites (CuFe$_2$O$_4$ and ZnFe$_2$O$_4$) are novel spinel ferrites that exhibit a crystal structure of cubic close-packed [15–17].

Pure ferrite nanoparticles of CuFe$_2$O$_4$ and ZnFe$_2$O$_4$, as well as mixed Cu–Zn ferrite nanoparticles, are synthesized

✉ Ahmad I. Ayesh
  ayesh@qu.edu.qa

1 Department of Chemistry, Khalifa University, Abu Dhabi, United Arab Emirates

2 Department of Mathematics, Statistics and Physics, Qatar University, P. O. Box 2713, Doha, Qatar

3 Department of Chemical Engineering, Khalifa University, Abu Dhabi, United Arab Emirates

4 Center for Sustainable Development, Qatar University, P. O. Box 2713, Doha, Qatar

in this work. The nanoparticles' size, composition, crystal structure, electrical characteristics, and gas sensing properties are examined. The nanoparticles are produced following the sol–gel auto-combustion technique. Scanning electron microscopy (SEM) is utilized to investigate the morphology and composition of nanoparticles. Their composition and structure are further confirmed by Fourier transform infrared spectroscopy (FTIR) and X-ray diffraction (XRD). The synthesized nanoparticles are used to fabricate conductometric gas sensors that are tested for their response to H_2S and H_2 gases. The results reveal that $CuFe_2O_4$ nanoparticles are the best in terms of their sensitivity to H_2S gas. The produced sensors are simple to fabricate with reasonable cost, and their nanoparticles are reusable since they are magnetic nanoparticles. They also have low operational power requirement; thus, they can be considered for practical applications.

2 Experimental

2.1 Materials

Ferric nitrate salt ($Fe(NO_3)_3 \cdot 9H_2O$), copper nitrate salt ($Cu(NO_3)_2 \cdot 3H_2O$), zinc nitrate salt ($Zn(NO_3)_2 \cdot 6H_2O$), citric acid ($C_6H_8O_7 \cdot H_2O$), ammonium hydroxide (NH_4OH), poly(vinyl alcohol) (PVA) (molecular weight 61,000 g/mol), and glycerol with purity of 99.5% were purchased from Sigma-Aldrich. Double distilled water was utilized for all synthesis.

2.2 Synthesis of nanoparticles

Pure ferrites of $ZnFe_2O_4$ and $CuFe_2O_4$ as well as a mixed ferrite of $Zn_{0.5}Cu_{0.5}Fe_2O_4$ were synthesized by the sol–gel auto-combustion method. Precise quantities of ferric nitrates ($Fe(NO_3)_3 \cdot 9H_2O$) and the corresponding metal nitrate salts [$Cu(NO_3)_2 \cdot 3H_2O$ and $Zn(NO_3)_2 \cdot 6H_2O$] were dissolved individually in distilled water based on their molar proportion. $C_6H_8O_7 \cdot H_2O$ was then introduced to the nitrate solution with continuous stirring at 80 °C. The experimental molar ratio of ferric nitrate, metal nitrate, and citric acid was 2:1:3, respectively. The pH value was adjusted to 8.0 by introducing NH_4OH gradually to the solution. The acquired solution was then evaporated to obtain a viscous gel that was kept overnight at room temperature. The gel product was then burned by a self-propagating auto-combustion reaction that produced a powder that was ash-like. Hereafter, the obtained powder is referred to as "as-prepared." Further, heat annealing was performed for the as-prepared samples at 500 °C and 750 °C for 5 h.

2.3 Sensor fabrication

A viscous polymeric solution made of PVA and glycerol was used as a binder for nanoparticles on a glass substrate. A 10 wt% of PVA solution was prepared by dissolving 10 g of PVA granules in 100 mL of distilled water at 80 °C with continuous stirring. After being completely dissolved, 50 mL of ethanol was introduced with continuous heating and stirring until a viscous solution was obtained. Glycerol was added at a concentration of 5 wt% to 10 g of PVA solution. Glass slides that are $10 \times 10 mm^2$ each were washed in a sonicator bath by means of acetone, ethanol, and distilled water. A small amount of this viscous polymeric solution was cast on the glass substrate, where it acted as a binder. Around 1 mg of nanoparticles were spared on the substrate and then packaged by a drop of the PVA solution. The sample was then heated at 80 °C for two hours.

2.4 Characterization

A scanning electron microscope FEI (QUANTA-250) with an energy-dispersive x-ray spectroscopy attachment (EDS) was used to determine the morphologies and compositions of the ferrite samples. A gold thin film was deposited on samples' surfaces before SEM and EDS tests to obtain sound resolution. A Bruker ALPHA-Platinum Fourier-transform infrared spectroscopy (FTIR) was utilized to characterize the samples in the range of 400-4000 cm^{-1}. The crystal structures of the prepared ferrites were determined by XRD in the 2θ angle range of 10°-80° using a PANalytical Powder Diffractometer (X'Pert PRO) with Cu-K_α radiation (1.5406 Å) as a radiation source. The crystallite sizes were calculated by Debye–Scherrer formula [18]:

$$D = \frac{K\lambda}{B cos\theta} \tag{1}$$

where K is Scherrer's constant (set to 0.89), λ is the wavelength of the XRD radiation, θ is the angle of diffraction, B is the XRD peak intensity with full width at half maximum of 2θ profile, and D is the nanoparticle size in nm [19–21].

For electrical characterization, a copper holder with a pair of parallel linear electrodes that were 1.5 mm apart was placed on top of the sample. The parallel electrodes were connected electrically to wires (glued by silver paste) to enable current–voltage (I(V)) and sensitivity measurements. All I(V) and sensitivity measurements were taken on a temperature controlled stage fixed in a Teflon chamber before gas exposure at 25, 80, and 140 °C in a voltage range of −50–50 V using a Keithley Instruments source

measurement unit (SMU-236). The temperature of the sample was measured and controlled by a thermocouple (K-type) fixed on the sample surface. The sample was then cooled down to 25 °C, and H$_2$ gas sensing measurements were taken at the same temperatures. Next, the sample was cooled down again to 25 °C and H$_2$S gas sensing measurements were established. The gas sensitivity tests were performed inside the Teflon chamber where the target gas was diluted with air by Bronkhorst mass flow meters. Herein, a gas electrical current response was measured across each sensor at a constant voltage.

3 Results and discussion

The SEM images of the as-prepared and annealed ferrite materials are presented in Fig. 1. The nanoparticles' sizes are presented in Table 1 which reveals that the
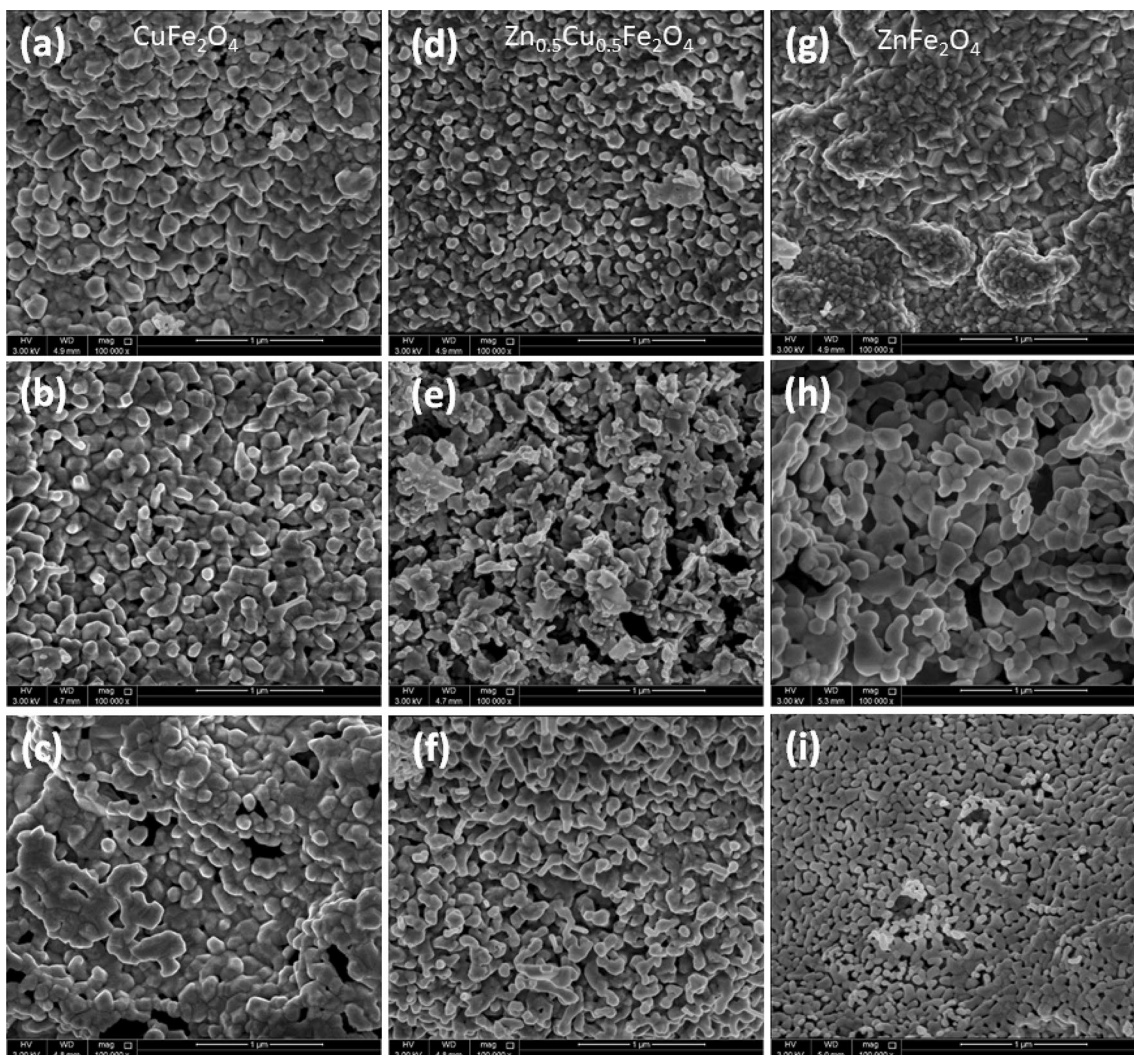
Fig. 1 SEM images of: **a–c** CuFe$_2$O$_4$, **d–f** Zn$_{0.5}$Cu$_{0.5}$Fe$_2$O$_4$, and **g–i** ZnFe$_2$O$_4$ nanoparticles. The images in **a**, **d**, and **g** are as-prepared; **b**, **e**, and **h** are annealed at 500 °C; and **c**, **f**, and **i** are annealed at 750 °C

Table 1 Nanoparticles' sizes as determined from SEM and XRD measurements

Sample	D$_{as-prepared}$ (nm)		D$_{500°C}$ (nm)		D$_{750°C}$ (nm)	
	SEM	XRD	SEM	XRD	SEM	XRD
CuFe$_2$O$_4$	50	50 ± 10	60	58 ± 12	70	69 ± 14
Zn$_{0.5}$Cu$_{0.5}$Fe$_2$O$_4$	40	42 ± 9	50	52 ± 11	60	65 ± 14
ZnFe$_2$O$_4$	30	38 ± 8	40	44 ± 9	50	48 ± 10

sizes increase in general with annealing. The images and Table 1 demonstrate that nanoparticles' sizes decrease with increasing the Zn content. Altering the Zn:Cu ratios in $Zn_xCu_{1-x}Fe_2O_4$ samples (where x = 0, 0.5, and 1) can be clearly observed in the SEM images. Figure 2 shows the EDS images of the three samples and a table of their average composition (the average in the table is determined from three different measurements). The EDS results clearly confirm the composition of the produced nanoparticles with ratios close to the theoretical values. Figures 1 and 2 reveal the reflection of the variation in the chemical composition of the ferrites on their surfaces' morphology.

XRD is employed to characterize the phase and crystallinity of the as-prepared and annealed for pure ($ZnFe_2O_4$ and $CuFe_2O_4$) and mixed ($Cu_{0.5}Zn_{0.5}Fe_2O_4$) ferrite samples. The XRD results of the ferrite samples are presented in Fig. 3. The XRD patterns of the as-prepared $ZnFe_2O_4$ and $CuFe_2O_4$, presented in Fig. 3, agree with JCPDS cards 79-1150 and 77-0010, respectively. These patterns show the distinctive reflection plans that confirm the spinel cubic structure, which are (111), (220), (311), (222), (400), (422), (511), (440), and (533) reflections [20]. All the peaks of the patterns of the as-prepared samples can be indexed as cubic phases of pure $ZnFe_2O_4$ and $CuFe_2O_4$ ferrites as well as cubic phases of mixed $Cu_{0.5}Zn_{0.5}Fe_2O_4$ ferrite. The figure
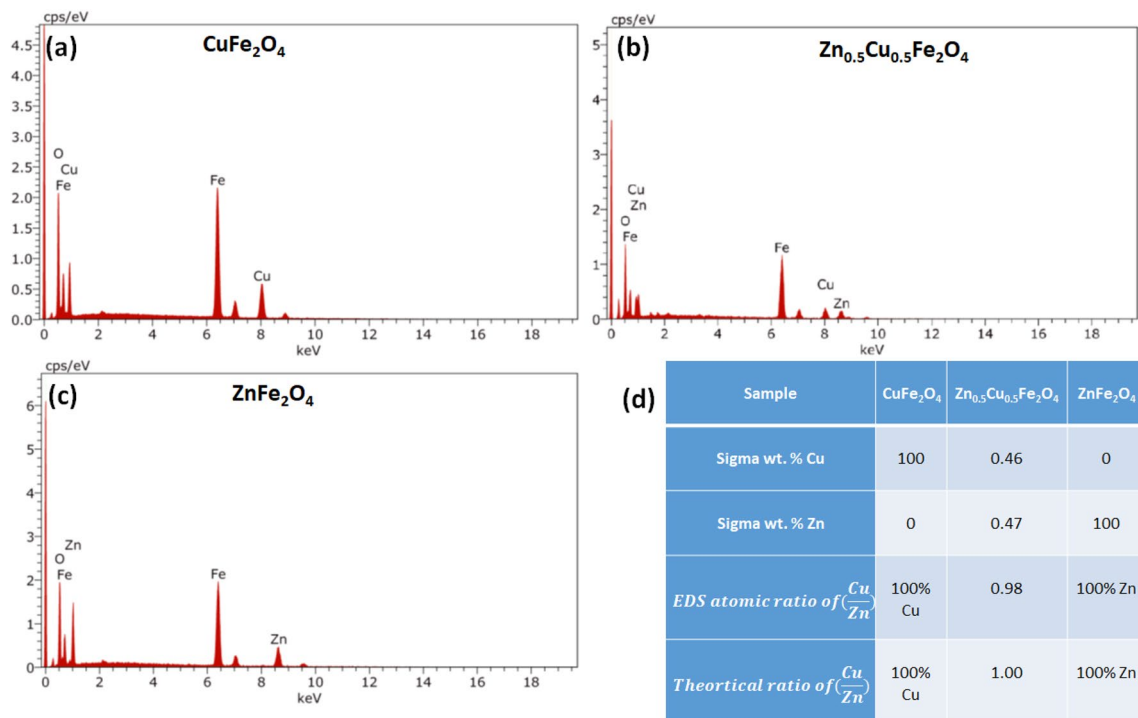

Fig. 2 EDS spectra of **a** $CuFe_2O_4$, **b** $Zn_{0.5}Cu_{0.5}Fe_2O_4$, and **c** $ZnFe_2O_4$ nanoparticles. The table in **d** presents a comparison of the theoretical and experimental wt% of Zn and Cu
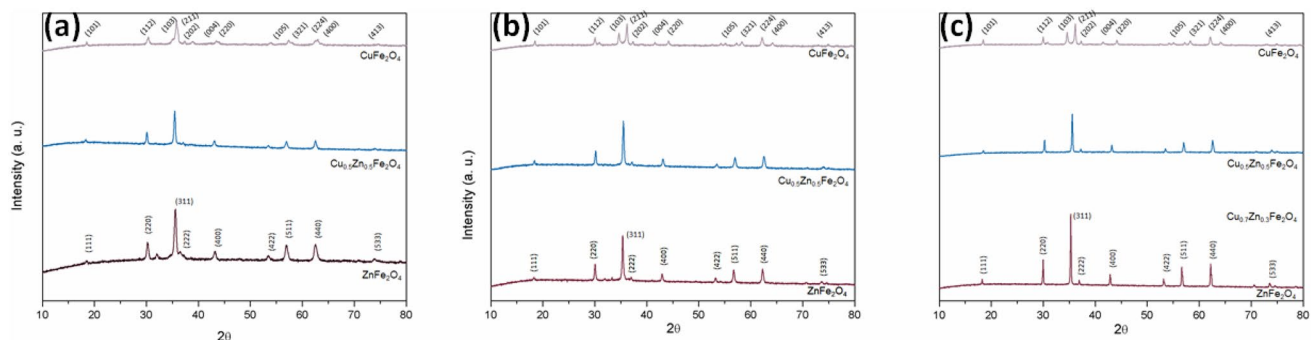

Fig. 3 XRD of $CuFe_2O_4$, $Zn_{0.5}Cu_{0.5}Fe_2O_4$, and $ZnFe_2O_4$ nanoparticles. **a** As-prepared, **b** annealed at 500 °C, and **c** annealed at 750 °C

also reveals the effect of annealing the ferrite samples. The crystallinity of these ferrites is observed to develop with sharp and intense peaks upon annealing. By increasing the annealing temperature up to 750 °C, the degree of crystallinity of the ferrites increases which indicates the high quality of the ferrites. Heat treatments of the ferrites are expected to affect their physicochemical properties. The disorder of ferrite surfaces is caused by oxygen vacancies and bond frustration at different sub-lattices on the surfaces. Thus, as the nanoparticle size decreases the disorder becomes more significant. However, the terminated unit cells of the surface are completed by the atmospheric oxygen when the ferrite undergoes heat treatment which reduces its surface strain/stress [22]. The XRD peak at around 35.5° is employed to determine the nanoparticles' sizes using the Debye–Scherrer formula (Eq. 1). The calculated sizes are presented in Table 1, and they are consistent with the sizes obtained from the SEM images. It should be noted here that the samples include size distributions and agglomerations of nanoparticles that reason disparity in the actual size estimation.

Figure 4 shows the FTIR spectra of the produced spinel ferrite nanoparticles along with pictures of the produced membranes Fig. 4a, c. All spectra exhibit a characteristic vibrational mode ν_T located around 530 cm^{-1} that is assigned to the stretching of the tetrahedral group complex (iron-oxygen ions) [23]. The ν_T mode values for the three types of nanoparticles are introduced in Table 2. The discrepancies in the ν_T mode values can be generated by the variation in the inter-nuclear distances of Fe^{+3}–O^{-2}. If the cation located in the lattice is shifted by a cation that exhibits a larger ionic radius, it causes an increase in the length of the bond that decreases the force constant for one site or lowers the repulsion among ions. This leads to a reduction in the electrostatic energy and, thus, to a lower wavenumber. The contrary will occur if the cation in the lattice is shifted by a cation of a smaller ionic radius. Table 2 reveals a shift in ν_T mode values toward reduced wavenumbers as the amount

Table 2 FTIR absorption band ν_T mode for CuFe$_2$O$_4$, ZnFe$_2$O$_4$ and Zn$_{0.5}$Cu$_{0.5}$Fe$_2$O$_4$ samples

Sample	ν_T (cm^{-1})		
	As-prepared	500 °C	750 °C
Cu Fe$_2$O$_4$	531	533	533
ZnFe$_2$O$_4$	529	525	524
Zn$_{0.5}$ Cu$_{0.5}$ Fe$_2$O$_4$	530	529	526

of Zn ions increases. This shift to low frequencies demonstrates that the force constant for Fe^{+2}–O^{-2} is reducing in Zn$_x$Cu$_{1-x}$Fe$_2$O$_4$ in the order of x = 1, 0.5, and 0.

Figure 5 shows the I(V) characteristics measured at 25 °C of the three types of nanoparticles as a function of annealing temperatures. The figure reveals a decrease in the electrical resistance $\left(R = \frac{V}{I} \right)$ with annealing temperature. For CuFe$_2$O$_4$ nanoparticles, the resistances of the as-prepared and 500 °C annealed samples are close, while the resistance of the sample annealed at 750 °C is lower. For ZnFe$_2$O$_4$ nanoparticles, the resistances of both samples annealed at 500 °C and 750 °C are similar and lower than that of the as-prepared sample. This indicates that annealing CuFe$_2$O$_4$ sample at 500 °C is not sufficient to enhance its electrical conductivity, while it is sufficient to enhance its electrical conductivity of the ZnFe$_2$O$_4$ sample. The Zn$_{0.5}$Cu$_{0.5}$ Fe$_2$O$_4$ sample must be annealed at 500 °C to enhance its electrical conductivity.

The response to H$_2$S and H$_2$ gases of the produced sensors is tested as a function of gas concentration and temperature. A gas response test is established by applying a constant voltage across the electrodes of a sensor and measuring the change in the electrical current during gas exposure as shown schematically in Fig. 6a. The insets of Fig. 6b show the gas test chamber. A typical electrical current response signal is shown in Fig. 6b. The figure reveals
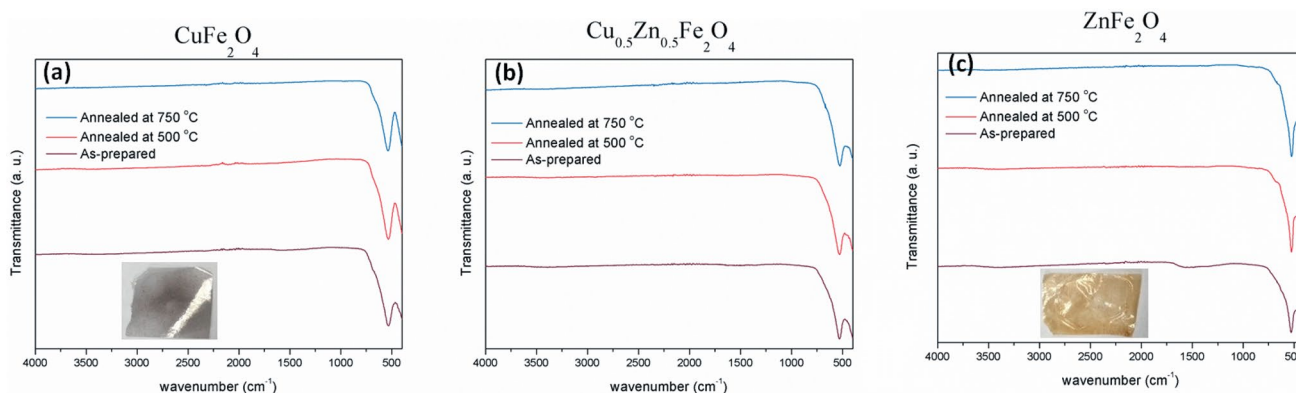

Fig. 4 FTIR spectra of **a** CuFe$_2$O$_4$, **b** Zn$_{0.5}$Cu$_{0.5}$Fe$_2$O$_4$, and **c** ZnFe$_2$O$_4$ nanoparticles. Each figure presents the FTIR spectra of nanoparticles as-prepared, annealed at 500 °C, and annealed at 750 °C. The insets in **a** and **c** are pictures of the produced membranes
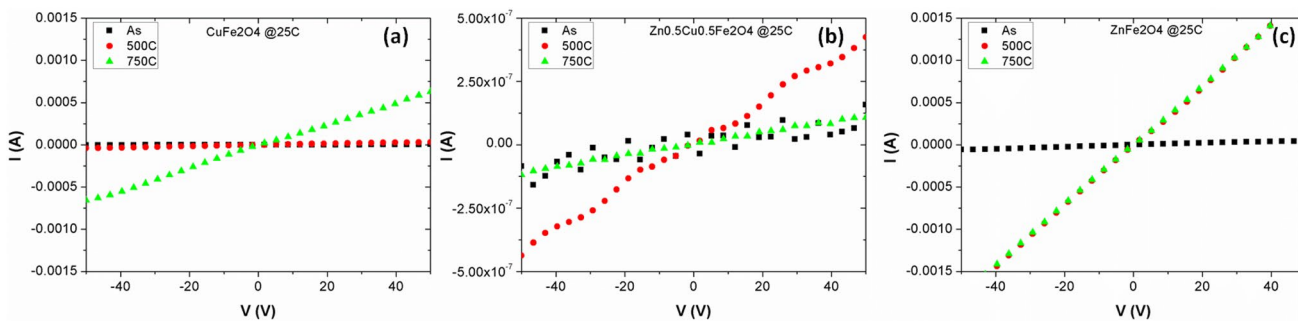
Fig. 5 Effect of annealing of nanoparticles on I(V) characteristics for **a** $CuFe_2O_4$, **b** $Zn_{0.5}Cu_{0.5}Fe_2O_4$, and **c** $ZnFe_2O_4$
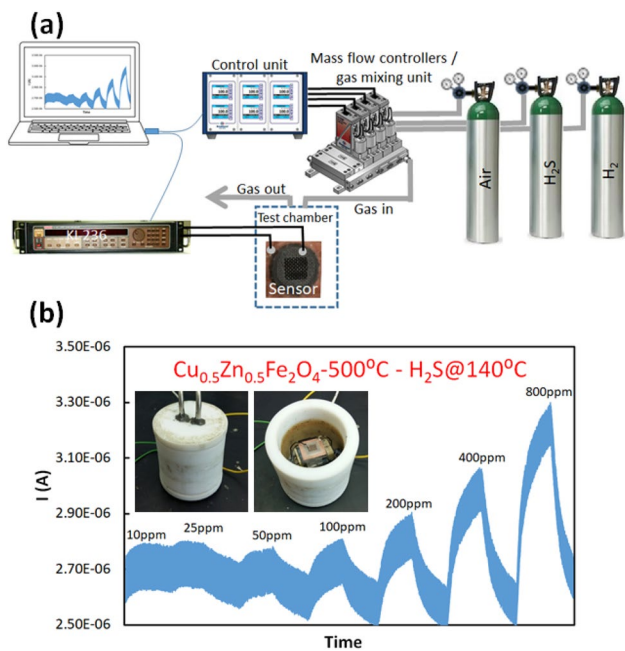

Fig. 6 **a** Schematic diagram of the gas sensing setup. **b** Electrical current measurement signal for H_2S gas at 140 °C for a sensor based on $Zn_{0.5}Cu_{0.5}Fe_2O_4$ nanoparticles. The insets in **b** are pictures of the gas test chamber

that the electrical current increases upon exposure to H_2S gas with a value that is proportional to the gas concentration. The electrical current signal returns to its reference value once the flow of H_2S gas is stopped and the chamber space is "washed" with air. If I_{ref} and I_{gas} represent the electrical current of the reference (without gas) and upon exposure to the target gas, respectively, the sensor gas response can be defined as:

$$S = \left| \frac{I_{gas} - I_{ref}}{I_{ref}} \right| = \frac{|\Delta I|}{I_{ref}} \tag{2}$$

Figure 7 shows H_2S gas sensors' response as a function of the sensor temperature and gas concentration. The figure reveals, in general, an increase in sensors' response with increasing the temperature and gas concentration. The sensor based on $CuFe_2O_4$ nanoparticles exhibited a higher response toward H_2S than sensors that contain Zn. The sensors are sensitive to H_2S gas at low temperatures (25 °C) and low concentrations of 10 ppm. The sensors' response toward H_2 gas as a function of sensor temperature and gas concentration is presented in Fig. 8. The figure reveals lower sensors' responses toward H_2
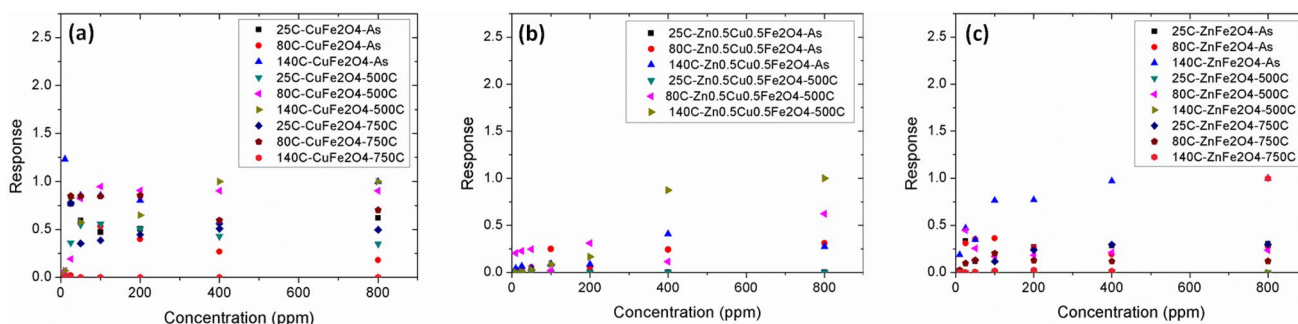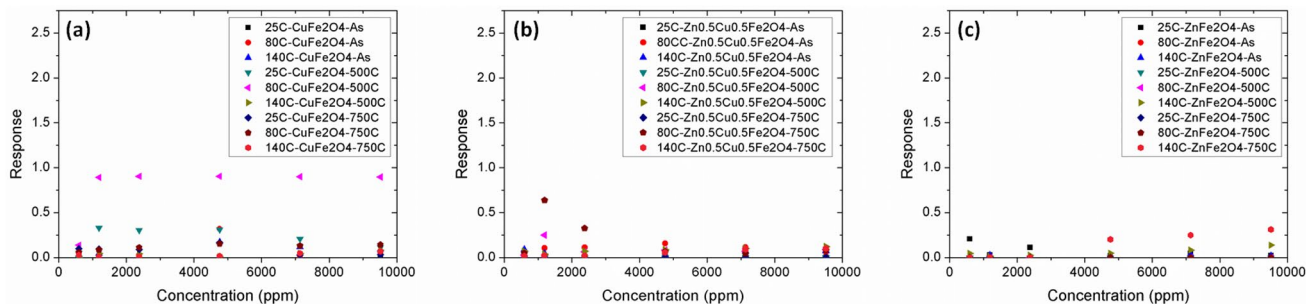

Fig. 7 Response of the fabricated sensors for H_2S gas as a function of gas concentration at different temperatures for sensors based on: **a** $CuFe_2O_4$, **b** $Zn_{0.5}Cu_{0.5}Fe_2O_4$, and **c** $ZnFe_2O_4$ nanoparticles

Fig. 8 Response of the fabricated sensors for H$_2$ gas as a function of gas concentration at different temperatures for sensors based on: **a** CuFe$_2$O$_4$, **b** Zn$_{0.5}$Cu$_{0.5}$Fe$_2$O$_4$, and **c** ZnFe$_2$O$_4$ nanoparticles
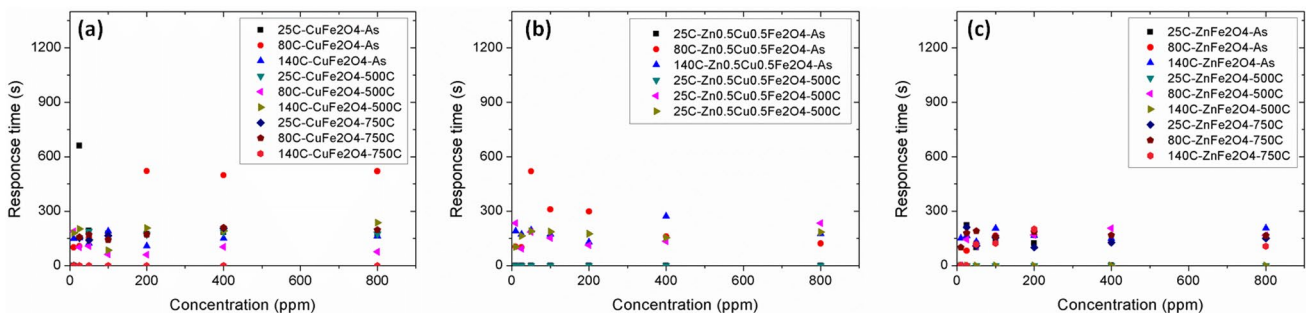

Fig. 9 Dependence of sensors' response time on H$_2$S gas concentration and temperature for sensors based on: **a** CuFe$_2$O$_4$, **b** Zn$_{0.5}$Cu$_{0.5}$Fe$_2$O$_4$, and **c** ZnFe$_2$O$_4$ nanoparticles

gas as compared with H$_2$S gas. The gas concentration for H$_2$ is different than that of H$_2$S due to the different gas responses.

The response time of a sensor is typically the time required for electrical current response to achieve 90% of its full value. Figure 9 presents the response time as a function of temperature and H$_2$S concentration. The figure reveals close values of response time regardless of the temperature and gas concentration. The average value of response time over different temperatures and gas concentrations is 170 ± 82 s. The error is estimated as one standard deviation. The response time is reasonable in comparison with previous reports for similar sensors [24, 25].

The produced sensors are sensitive to H$_2$S at 25 °C that specifies their low power requirements as well as safe operation. The response of the sensors that contain Cu toward H$_2$S is higher than that of H$_2$ indicating their selectivity to H$_2$S gas. The large surface-to-volume ratio of nanoparticles enables enhanced gas response as compared with their bulk substitute. The response signal saturation at high gas concentrations can be designated to adsorption of H$_2$S gas on most nanoparticles' surfaces reactive sites. The response of spinel ferrite nanoparticles that contain Cu to H$_2$S can be assigned to the production of charge carriers as a result of adsorption of oxygen species such as O$^-$ and

O^{2-} at the surface of reactive sites [26, 27]. This process can be described as [28]:

$$H_2S + 3O^-_{(ads)} \rightarrow H_2O + SO_2 + 3e^- \tag{3}$$

$$H_2S + 3O^{2-}_{(ads)} \rightarrow H_2O + SO_2 + 6e^- \tag{4}$$
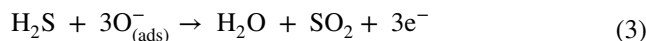
Hence, the increase in electrical current signals of sensors upon exposure to H$_2$S gas can be assigned to the increase of the concentration of free electrons as described by Eqs. 3 and 4. Once H$_2$S gas is stopped and the sensor is washed by air, the production of free electrons is stopped and, thus, the electrical current signal decreases back to its reference. The sensing mechanism of H$_2$S is a reversible process that enables using the sensor for repeatable sensing tests.

Copper-based spinel ferrites react with H$_2$S leading to the production of chalcopyrite [29, 30] by the reduction of CuFe$_2$O$_4$ and formation of an intermediate compound CuFeO$_2$ and then CuFeS$_2$ as described by the following reaction [29, 30]:

$$CuFeO_2 + H_2S \rightarrow CuFeS_2 + H_2O \tag{5}$$
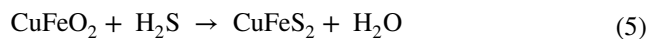
The produced CuFeS$_2$ layer represents a small barrier layer for the ejected electrons on the nanoparticles' surface

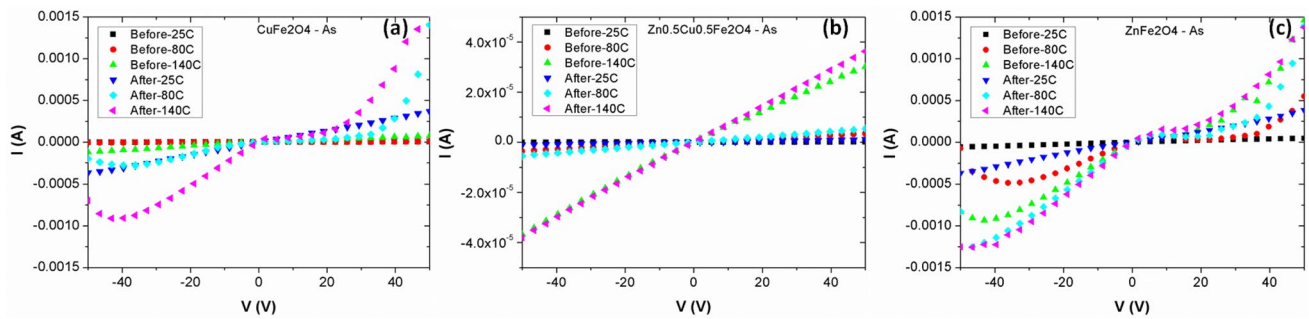**Fig. 10** Effect of gas exposure on I(V) characteristics at different temperature for as-prepared: **a** $CuFe_2O_4$, **b** $Zn_{0.5}Cu_{0.5}Fe_2O_4$, and **c** $ZnFe_2O_4$ nanoparticles

since it exhibits higher conductivity than $CuFe_2O_4$. The electrons do not require high energy to pass the barrier and move within the nanoparticles' network; hence, those sensors are functional at room temperature. Furthermore, electrons are free to move within the nanoparticles network that increase the electrical current signal in comparison with the case of air exposure only. Upon exposing the sensor to air, $CuFeS_2$ oxidizes and forms $CuFe_2O_4$ that exhibits a lower conductivity than $CuFeS_2$. The functionality of the produced sensors is not sensitive to the ambient humidity because of the production of H_2O molecules on the surface of the metal-oxide nanoparticles upon gas adsorption (Eqs. 3, 4, and 5).

The I(V) characteristics of the three as-prepared ferrite samples before and after exposure to H_2S gas are presented in Fig. 10 which reveals two common features of the three samples: negative temperature coefficient of resistivity (i.e., decrease in resistance with temperature) and increase in electrical conductivity after exposure to H_2S gas. The nanoparticles annealed at 500 °C and 750 °C exhibit a similar behavior. Spinel ferrite nanoparticles are semiconducting metal-oxide materials; thus, they are expected to reveal the negative temperature coefficient of resistivity with temperature [31]. The increase in electrical conductivity after exposure to H_2S gas supports the suggested sensing mechanism presented in Eq. 5 that leads to the formation of metallic $CuFeS_2$ that exhibits higher electrical conductivity than the metal-oxide spinel ferrites.

4 Conclusion

Metal-oxide spinel ferrite nanoparticles of a composition $Zn_xCu_{1-x}Fe_2O_4$ (x = 0, 0.5, and 1) were synthesized by the sol–gel auto-combustion technique and were annealed at elevated temperatures. The nanoparticles exhibit average sizes between 30 and 70 nm with cubic structures. The nanoparticles were tested for their H_2 and H_2S sensitivity at different temperatures. Copper ferrite nanoparticles revealed best sensitivity and selectivity to the H_2S gas.

This improved response to H_2S gas is explained in terms of the production of metallic $CuFeS_2$ that has a lower electrical resistivity compared to the semiconducting $CuFe_2O_4$. The fabricated sensors are safe to operate since they are functional at low temperatures, which also leads to low operating power requirements. Hence, they represent suitable candidates for the sensing elements in practical portable sensors.

References

1. P.P. Hankare, S.D. Jadhav, U.B. Sankpal, R.P. Patil, R. Sasikala, I.S. Mulla, Gas sensing properties of magnesium ferrite prepared by co-precipitation method. J. Alloy. Compd. **488**, 270–272 (2009)
2. H. Kimura, Physiological role of hydrogen sulfide and polysulfide in the central nervous system. Neurochem. Int. **63**, 492–497 (2013)
3. M.M. Alsaif, M.R. Field, B.J. Murdoch, T. Daeneke, K. Latham, A.F. Chrimes, A.S. Zoolfakar, S.P. Russo, J.Z. Ou, K. Kalantar-Zadeh, Substoichiometric two-dimensional molybdenum oxide flakes: a plasmonic gas sensing platform. Nanoscale **6**, 12780–12791 (2014)

4. A. Ahmadivand, S. Golmohammadi, N. Pala, Fano resonances in plasmonic aluminum nanoparticle clusters for precise gas detection: Ultra-sensitivity to the minor environmental refractive index perturbations. Photonics Nanostruct-Fundam. Appl. **13**, 97–105 (2015)

5. W. Wei, J. Nong, Y. Zhu, G. Zhang, N. Wang, S. Luo, N. Chen, G. Lan, C.-J. Chuang, Y. Huang, Graphene/Au-enhanced plastic clad silica fiber optic surface plasmon resonance sensor. Plasmonics **13**, 483–491 (2018)

6. F.E. Kruis, H. Fissan, A. Peled, Synthesis of nanoparticles in the gas phase for electronic, optical and magnetic applications—a review. J. Aerosol Sci. **29**, 511–535 (1998)

7. A.I. Ayesh, S.T. Mahmoud, S.J. Ahmad, Y. Haik, Novel hydrogen gas sensor based on Pd and SnO2 nanoclusters. Mater. Lett. **128**, 354–357 (2014)

8. G. Korotcenkov, The role of morphology and crystallographic structure of metal oxides in response of conductometric-type gas sensors. Mater. Sci. Eng. R: Rep. **61**, 1–39 (2008)

9. H. Yan, P. Song, S. Zhang, Z. Yang, Q. Wang, Facile synthesis, characterization and gas sensing performance of ZnO nanoparticles-coated MoS2 nanosheets. J. Alloy. Compd. **662**, 118–125 (2016)

10. N. Barsan, D. Koziej, U. Weimar, Metal oxide-based gas sensor research: How to? Sens. Actuators B: Chem. **121**, 18–35 (2007)

11. A.I. Ayesh, Z. Karam, F. Awwad, M.A. Meetani, Conductometric graphene sensors decorated with nanoclusters for selective detection of Hg2+ traces in water. Sens. Actuators B: Chem. **221**, 201–206 (2015)

12. A.I. Ayesh, A.F.S. Abu-Hani, S.T. Mahmoud, Y. Haik, Selective H2S sensor based on CuO nanoparticles embedded in organic membranes. Sens. Actuators B: Chem. **231**, 593–600 (2016)

13. T.P. Sumangala, C. Mahender, A. Barnabe, N. Venkataramani, S. Prasad, Structural, magnetic and gas sensing properties of nanosized copper ferrite powder synthesized by sol gel combustion technique. J. Magn. Magn. Mater. (2016). https://doi.org/10.1016/j.jmmm.2016.02.053

14. A.I. Ayesh, A.A. Alyafei, R.S. Anjum, R.M. Mohamed, M.B. Abuharb, B. Salah, M. El-Muraikhi, Production of sensitive gas sensors using CuO/SnO 2 nanoparticles. Appl. Phys. A **125**, 550 (2019)

15. S. Tao, F. Gao, X. Liu, O. Toft Sørensen, Preparation and gas-sensing properties of CuFe2O4 at reduced temperature. Mater. Sci. Eng. B **77**, 172–176 (2000)

16. M.A. Amer, T. Meaz, A. Hashhash, S. Attalah, F. Fakhry, Structural phase transformations of as-synthesized Cu-nanoferrites by annealing process. J. Alloy. Compd. **649**, 712–720 (2015)

17. E. Ranjith Kumar, R. Jayaprakash, S. Kumar, The role of annealing temperature and bio template (egg white) on the structural, morphological and magnetic properties of manganese substituted MFe2O4 (M=Zn, Cu, Ni, Co) nanoparticles. J. Magn. Magn. Mater. **351**, 70–75 (2014)

18. L.A. Al-Sulaiti, B. Salah, A.I. Ayesh, Investigation of flexible polymer-Tl2O3 nanocomposites for x-ray detector applications. Appl. Surf. Sci. **489**, 351–357 (2019)

19. A.I. Ayesh, M.A. Haija, A. Shaheen, F. Banat, Spinel ferrite nanoparticles for H2S gas sensor. Appl. Phys. A **123**, 682 (2017)

20. M.A. Haija, A.I. Ayesh, S. Ahmed, M.S. Katsiotis, Selective hydrogen gas sensor using CuFe2O4 nanoparticle based thin film. Appl. Surf. Sci. **369**, 443–447 (2016)

21. A.R. Said, K. Said, F. Awwad, N.N. Qamhieh, S.T. Mahmoud, M.A. Meetani, S. Tariq, A.I. Ayesh, Design, fabrication, and characterization of Hg2+ sensor based on graphite oxide and metallic nanoclusters. Sens. Actuators A-Phys. **271**, 270–277 (2018)

22. L. Ai, J. Jiang, Influence of annealing temperature on the formation, microstructure and magnetic properties of spinel nanocrystalline cobalt ferrites. Curr. Appl. Phys. **10**, 284–288 (2010)

23. Y. Zhang, Q. Shi, J. Schliesser, B.F. Woodfield, Z. Nan, Magnetic and thermodynamic properties of nanosized Zn ferrite with normal spinel structure synthesized using a facile method. Inorg. Chem. **53**, 10463–10470 (2014)

24. A.F. Abu-Hani, S.T. Mahmoud, F. Awwad, A.I. Ayesh, Design, fabrication, and characterization of portable gas sensors based on spinel ferrite nanoparticles embedded in organic membranes. Sens. Actuators B: Chem. **241**, 1179–1187 (2017)

25. E. Ranjith Kumar, P. Siva Prasada Reddy, G. Sarala Devi, S. Sathiyaraj, Structural, dielectric and gas sensing behavior of Mn substituted spinel MFe2O4 (M=Zn, Cu, Ni, and Co) ferrite nanoparticles. J. Magn. Magn. Mater. **398**, 281–288 (2016)

26. F.-N. Meng, X.-P. Di, H.-W. Dong, Y. Zhang, C.-L. Zhu, C. Li, Y.-J. Chen, Ppb H2S gas sensing characteristics of Cu2O/CuO sub-microspheres at low-temperature. Sens. Actuators B: Chem. **182**, 197–204 (2013)

27. A.H. Reshak, S. Auluck, Adsorbing H2S onto a single graphene sheet: A possible gas sensor. J. Appl. Phys. **116**, 103702 (2014)

28. A.I. Ayesh, R.E. Ahmed, M.A. Al-Rashid, R.A. Alarrouqi, B. Saleh, T. Abdulrehman, Y. Haik, L.A. Al-Sulaiti, Selective gas sensors using graphene and CuO nanorods. Sens. Actuators A **283**, 107–112 (2018)

29. M. Flytzani-Stephanopoulos, S. Tamhankar, G. Gavalas, P Sharma, in *High-temperature regenerative removal of H2S by porous mixed metal-oxide sorbents*. Abstracts of papers of the American Chemical Society, vol. 190, no. 1155 (American Chemical Society, Washington, DC, 1985)

30. M.A. Haija, G. Basina, F. Banat, A.I. Ayesh, Adsorption and gas sensing properties of CuFe2O4 nanoparticles. Mater. Sci. Poland **37**(2), 289–295 (2019)

31. M.A. Haija, A.F.S. Abu-Hani, N. Hamdan, S. Stephen, A.I. Ayesh, Characterization of H2S gas sensor based on CuFe2O4 nanoparticles. J. Alloy. Compd. **690**, 461–468 (2017)